Surface Modification of Powders and Nanostructure Deposition in the Afterglow of a Low Power Barrier Discharge at Atmospheric Pressure

A. Sonnenfeld[*], P. Reichen[**], and P. Rudolf von Rohr[***]

ETH Zurich, Institute of Process Engineering, Sonneggstrasse 3, 8092 Zürich, Switzerland
[*] sonnenfeld@ipe.mavt.ethz.ch
[**]patrick.reichen@ipe.mavt.ethz.ch
[***]philippr@ethz.ch

ABSTRACT

The generation of solid-state sphere-like nanostructures from an organosilicon precursor at atmospheric pressure is investigated with the prospect of improving powder flowabilty by the attachment of nanoscopic spacers to the powder particles`surface. An atmospheric pressure plasma discharge is used for remote surface modification. The setup effectively separates the discharge zone, where the active gassphase species are created from the deposition or afterglow zone, in which the chemical reactions of the active species occur. As a first step, the nanoparticle formation from Ar/O_2 or a He/O_2 atmospheric pressure plasma with tetramethylsilane as monomer added to the afterglow is investigated. The influence of the total gas glow rate and oxygen content on the formation of SiO_x particles is studied. The morphology of created nanostructures is investigated by electron microscopy and their chemical structure is analyzed by Fourier transform infrared (FTIR) spectroscopy

Keywords: plasma, dielectric barrier discharge, powder flowability, remote treatment, non-equilibrium

1 INTRODUCTION

For food, chemical and pharmaceutical applications, plasma surface engineering atrracts increasing attention with respect to the processing of powders. Here, a classical handling problem is the poor flow behaviour of dry, cohesive powders. For conveying and processing of fine powders, which is often encountered in the pharmaceutical and chemical industry, especially an adequate flow behaviour is required. Admixtures of nanoscopic so-called glidants, and their attachement to the surfaces by means of long-term mixing is a common mean of improving the powder flowability [1]. However, plasma enhanced chemical vapor deposition allows rapid improvement of the flow behaviour of dry powders by the formation and simultaneous attachment of nanoparticles to the substrate particle surface. The depositeted nanoparticles reduce the Van der Waals forces between the powder particles and thus improve the flowability of the particles as it has already been shown for low pressure plasmas. Atmospheric pressure non-equilibrum discharges are generally seen to be more cost-effective plasma sources. In this respect the direct treatment by means of atmospheric barrier discharges (BD) has been proposed for the improvement of surface wettability. However a drawback of the direct plasma treatment is obvious: Particle-wall interactions increases the risk of equipment clogging in a typical BD setup.

In this work, an atmospheric pressure micro-barrier discharge is investigated, which allows a remote treatment of powder particles. The results presented in this Conference Proceeding correspond to the paper orginally published in [2].

2 EXPERIMENTAL

2.1 BD Setup

The principle of the remote-BD operation in the single channeld device (SCD) is sketched in Figure 1(*a*). The BD occurs in a conically converging flow channel of gap height g = 1 mm. The channel is incorporated into a sandwich of two PMMA sheets, which are bonded with chloroform on top of each other. The lower PMMA sheet is d = 1 mm thick. Prior to bonding, the flow channel contour was machined into the upper 2mm thick sheet. The channel has a convergence angle of 16° and a total length of 37 mm along its centre line. With respect to the rectangular high-voltage electrode (30 × 15 mm^2), the discharge zone occupies a trapezoidal area of 193 mm^2 in the flow channel. As such, the gas flow enters the discharge zone at a cross-section of 10 mm × g and exits it at a crosssection of 2 mm × g. In order to prevent arcing between the electrodes, the entire electrode arrangement is cast in an epoxy resin. For the same reason, a recess length of 4mm is provided between the end of the discharge zone and the actual channel outflow. Here, the afterglow expands from the channel cross-section of 1.4 mm × g into a half-cylinder space with the radius of 5mm (figure 1(*a*), right). For the sake of clarity, the respective casing of epoxy cast and polytetrafluoroethylene plates, delimiting the half-cylinder, are omitted in figure 1(*a*).

In the half-cylinder, carrier gas and BD gas flow are combined and directed downwards along the silicon wafer (12 mm × 30 mm) at position A (figure 1(*a*)). Perpendicular to the flow, another Si wafer is placed below the outflow (position B). Thus, the SCD mimics a channel of the multi

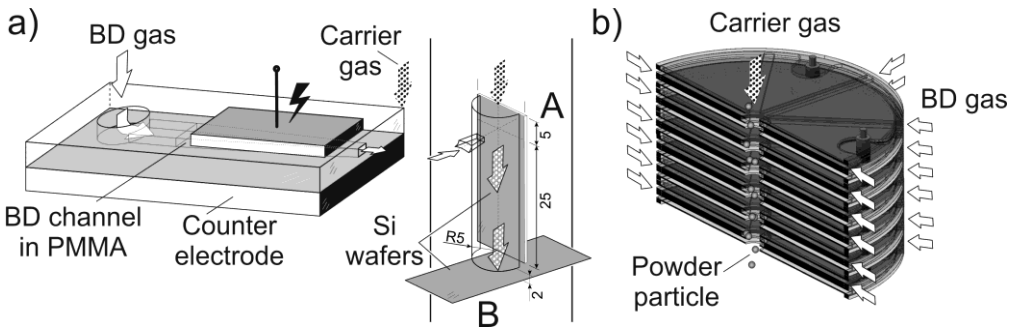

Figure 1: Sketch of (a) the remote–BD SCD setup initiation of TMS-based desposits at position A: Si wafer positioned opposite to the BD channel exit and position B: 25 mm downstream and (b) the MCD consisting of a stack of modules with 8 BD gas channels per module

channel device (MCD) (depicted in figure 1(*b*)) and allows simulating the flow conditions of the original MCD for remote-BD operation.

In the SCD, He or Ar (99.9999%) was used as the BD gas at flow rates of 2.8–3.5 slm with O_2 admixtures of 1–8 sccm. The organosilicon precursor tetramethylsilane (TMS, Fluka, CAS 75-76-3, purity >99%) was admixed to He or Ar as carrier gas and was introduced from the top of the device into the afterglow zone of the BD gas. The mass flow rate of TMS was controlled by a liquid flow controller to 0.27– 2.7 g h^{-1} prior to evaporation at 110 °C and mixing with the carrier gas, while the carrier gas flow rate was kept constant at 1.4 slm. The deposition time varied between 1 and 30 min.

A peak-to-peak (pp) voltage of 5 kV was applied at a frequency of 8 kHz resulting in a dissipated plasma power of 180–450 mW. In the case of the MCD (figure 1(*b*)), each BD nominally dissipates only 60 mW with Ar as the BD gas, mainly due to the lower applied driving frequency of 5 kHz. For the 64 channels of the MCD, this accumulates to a total dissipated power of 3.8 W. All power values were derived from the charge–voltage characteristics by means of the well-known Lissajous figure, which was acquired by a digital oscilloscope (LeCroy, WaveRunner 64Xi, 600 MHz). The applied voltage and the voltage drop across the serial charge-measuring capacitance of 1.49 nF were measured by means of a 1 : 1000 high-voltage probe (Tektronix, P6015) and a 1 : 100 voltage probe, respectively. For the treatment of high-density polyethylene (HDPE) powder in the MCD, 1.4 slm Ar as particle carrier gas and a total BD gas flow rate of 20–60 slm were applied, consisting of Ar with an admixture of 0–5 vol% O_2.

2.2 Contact angle measurement

The benzyl alcohol wettabilitiy improvement of HDPE powder (Schätti AG, Schätti Fix 1820) upon treatmend in the MCD was explored by a Krüss K100 tensiometer. A cylindrical glass tube (inner diameter 10mm 50 mm) with a filter at the bottom was cleaned and then filled with 800 +/- 5 mg powder, which was compacted by tapping 50 times with a Engsmann STAV II jolting volumeter. This procedure was repeated three times to derive a mean value of the benzyl alcohol contact angle (BACA), using Washburn method. Hexane was used as test liquid for the evaluation of the capillary constant of the powder bulk assuming full wetting.

2.3 FTIR

To determine SiO_x deposits on Si wafers FTIR spectroscopy was performed using a Perkin Elmer Sepctrum BX 2 spectrometer. For each spectrum, 32 scans were collected and averaged in the wavenumber range of 600-2200 cm^{-1} at 2 cm^{-1} resolution. Before the measurements the instrument was purged with nitrogen for at least 10 min to reduce interference with water and carbon dioxide from atmosphere

2.4 Scanning electron microscopy

SEM was carried out by a LEO 1530 Gemini (Carl Zeiss) with an acceleration voltage of the electron of 2kV and a focal length of 3.5 mm. The secondary electrons were detected for imaging. Samples were attached to mettalic sample holders by conductive double-sided adhesive carbon tape and sputter coated with a 4 nm thin platinum layer to prevent charging of the samples.

3 RESULTS

3.1 Wettability of powder treated in the MCD

In order to show the applicability of the remote-BD concept for the treatment of powders, the dependence of the mean BACA of HDPE on the total [Ar] + [O_2] flow rate is given in figure 2. Above a total flow rate of 40 slm, the decrease in BACA seems to level off. We see this incidence in the absence of dissipated plasma power by the MCD. Nevertheless, the BACA drops by about 15°. It is noteworthy that this decrease is achieved within an effective treatment time (residence time of the powder in the remote-BD zone) of less than 0.01 s. As showing the inset in figure 3, an optimum regarding the BACA is found

for an oxygen content of 0.25 vol% in the BD gas mixture within the limitations of the power supply. The very same optimum of contact angle with respect to the oxygen content in the BD gas of a similar MCD was also found when treating PMMA surfaces [3].

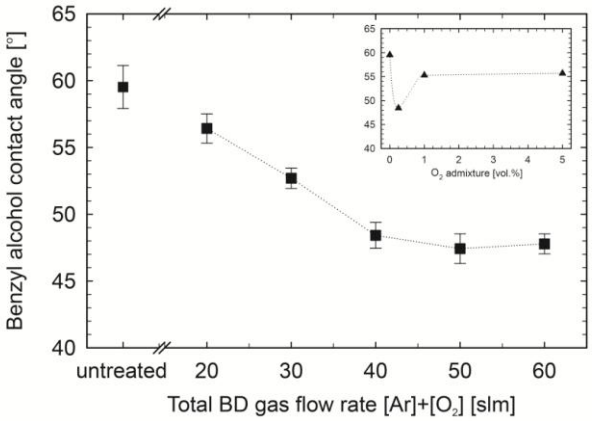

Figure 2: BACA of HDPE powder, treated in MCD at O_2 of 0.25%, versus total gas flow rate. Inset: BACA vs O_2

3.2 Chemical Characterization of TMS-based deposits

The FTIR spectra of SiOx coatings, deposited by the SCD from He–O2–TMS and an Ar–O2–TMS mixtures at positions A and B, are compared in the relevant spectral range 600–2200 cm−1 in figure 3, respectively. In general, the deposits obtained in the afterglow of the argon discharge appear not only thicker but also chemically different.

The most prominent absorption feature at 1200–1020 cm−1 can be assigned to the overlapping of the Si–O stretching in Si–O–Si (1064–1078 cm−1) and the asymmetric stretching of Si–O–C (1100–1165 cm−1 [4].

The presence of the Si–O stretching mode in Si–O–Si can be ascertained by its bending mode at 807 cm−1. Furthermore, typical absorption bands for the symmetric and asymmetric deformation of Si–C in Si–(CH3)x at 1260 and 1405 cm−1 are observed in the spectra for the argon BD deposits at both positions A and B.

With this, the deposits obtained by BD in the Ar–O2–TMS mixtures resemble typical features of organosilicon oxides obtained for instance by means of hexamethyldisiloxane (HMDSO).

For the He–O_2–TMS mixture, the absorption feature at 1200–1020 cm^{-1} is much weaker than that for Ar–O_2–TMS. Although the spectrum of deposits at position B appears similar to those obtained in Ar mixtures, the absorption of the Si–O bending mode in Si–O–Si at 807 cm^{-1} is completely missing. This suggests that no considerable amount of Si–O–Si is present. Therefore, the –CH_2– wagging in Si–CH2–Si (1030 cm^{-1}) must be considered here.

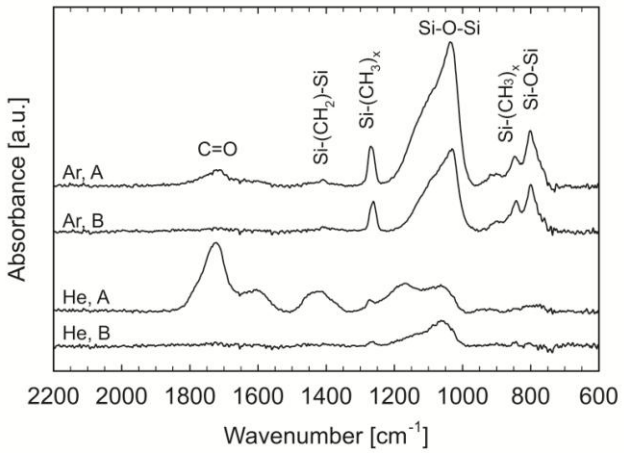

Figure 3 FTIR spectra of SiO coatings from Ar-O_2-TMS and He-O_2-TMS mixtures on Si wafers deposited at position A and B for 30 min, respectively

The coexistence of Si–O–C and Si–CH_2–Si structures is supported by the CH_2 scissor motion at 1400–1350 cm^{-1}. This band is especially prominent for deposits obtained from He–O_2–TMS at position A. The most prominent absorption of this spectrum at approximately 1720 cm^{-1} is ascribed to the C=O stretching vibration. Interestingly, this functionality is observed only at position A for both Ar and He. This fact may be related to atomic oxygen, which could be still present in the afterglow at position A but, due to its short lifetime, no longer at position B. The smaller absorption at 1600 cm^{-1}, which is observed for He, but hardly perceivable for Ar at position A, may be assigned to C=C. The less pronounced Si–O absorptions and the higher amounts of hydrocarbon structures found for He–O_2–TMS mixtures indicate a more polymeric character of the deposits compared with those from Ar–O_2–TMS mixtures. This suggests that more atomic oxygen is produced by the BD in Ar–O_2 than in He–O_2. It can be speculated that higher characteristic electron energies of the argon BD result in a higher rate of the electron impact dissociation of O_2 than in He mixtures.

Furthermore, VUV radiation, capable of dissociating O_2, must be considered. In argon BD, the production of Ar excimers (radiating at 126 nm) is very effective, while in He the predominant storage of energy in long-lived He metastables hinders the formation of significant quantities of VUV radiating species.

3.3 Morphological characterization of the TMS-based deposits

The first insight into the morphology of the deposits was obtained by SEM. Process times as short as the effective treatment time of powders did not result in recognizable deposits in the corresponding micrographs. Therefore, the deposition experiments were prolonged to the minute scale. The corresponding micrographs are exemplarily shown in

figure 4. Here, a difference concerning the Ar–O_2–TMS and the He–O_2–TMS deposition system can also be observed. For Ar–O_2–TMS at position A, particle-like structures of characteristic dimensions between 100 and 1000 nm can be observed in figure 4(*a*). This scale is already much larger than the aspired particle size, found beneficial for the improvement of powders [5].

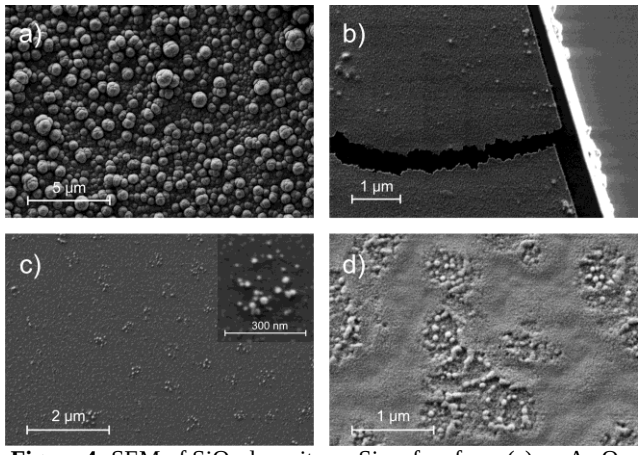

Figure 4: SEM of SiO_x deposits on Si wafers from (a) an Ar-O_2-TMS mixture at position A after a process time of10 min with 20000 fold magnification, (b) a He-O_2-TMS mixture at position A after a process time of 10 min with 50000 fold magnification, (c) a He-O_2-TMS mixture at position B after a process time of 1 min with 50000 fold magnification, and (d) a He-O_2-TMS mixture at position B after a process time of 10 min with 50000 fold magnification**.**

Since we assume the characteristic structures to grow further downstream the afterglow, the evaluation of the deposits at position B is discarded for the Ar–O_2–TMS systems. In contrast, for the He–O_2–TMS system very thin and smooth films are observed at position A even at a 2.5 times higher magnification of the SEM as shown in figure 4(*b*). In this case, the observation of the deposited film by SEM is only perceivable because of a breach running along the deposit, which is scratched purposely into the deposit for that reason. A clear influence of the process time is seen for deposits from He–O_2–TMS at position B. For 1 min, a nanoparticle-triggered island-like growth is initiated as depicted in figure 4(*c*). These nanospherical structures reveal characteristic dimensions of less than 100 nm. For an increased process time of 10 min, the characteristic size of these features is still in the nanometre range (figure 4(*d*)), but a coherent film consisting of these spherical structures seems to form, which is partially subjected to a heterogeneous overcoating

4 CONCLUSION

By means of a low plasma power BD, transient excited species are created inside the narrow volume of a single flow channel. It was shown that by admixing TMS to the atmospheric afterglow, remote homogeneous gas phase reactions result in the nucleation of solid-state nanoscopic particles of qualitatively different scale and chemistry with respect to the respective noble gas admixed to the BD.

Investigation of the deposits at different process times suggests that higher conversion rates are achieved in the case of Ar–O_2–TMS mixtures, leading to larger particles in the range 100–1000 nm. FTIR analysis shows that the respective deposits from the Ar–O_2–TMS mixtures on silicon wafers placed in the afterglow contain higher amounts of SiO_2-like structures than those obtained in He–O_2–TMS. In the case of He–O_2–TMS, the conversion rate is globally smaller, likely leading to a plasma polymer. The characteristic particle dimensions are clearly below 100 nm for both 1 and 10 min processing time. However, a coherent film consisting of these spherical structures is observed for the longer processing time, while island-like spots of nanoparticles are found after 1 min of processing.

Concerning the deposition location in the remote afterglow, a larger variety and higher fractions of oxygencontaining structures are observed in the FTIR spectra close to the exit of the BD gas into the afterglow (position A). This shows that the transfer of excited species (atomic oxygen) from the BD zone to the afterglow is well feasible by means of a high drift. The investigated deposits obtained about 25 mm downstream (position B) reveal that the conversion of TMS is incomplete and atomic oxygen formed in the BD is no longer taking part in this process.

ACKNOWLEDGMENT

Financial support by the Foundation Claude & Giuliana is gratefully acknowleged. This work was supported by ETH Research Grant ETH-08 08-1.

REFERENCES

[1] Sonnenfeld, A., et al., *Plasma Enhanced Chemical Vapor Deposition on Particulate Solid-State Materials for Improved Powder Processing.* Plasma Processes and Polymers, 2009. **6**(S1): p. S860-S863.

[2] Sonnenfeld, A., et al., *Nanostructure deposition in the afterglow of a low power barrier discharge.* Journal of Physics D-Applied Physics, 2011. **44**(7).

[3] Reichen, P., A. Sonnenfeld, and P.R.v. Rohr, *Remote Plasma Device for Surface Modification at Atmospheric Pressure.* Plasma Processes and Polymers, 2009. **6**(S1): p. S382-S386.

[4] Sonnenfeld, A., et al., *Deposition process based on organosilicon precursors in dielectric barrier discharges at atmospheric pressure-a comparison.* Plasmas and Polymers, 2001. **6**(4): p. 237-266.

[5] Sonnenfeld, A., et al., *Application of plasma surface treatment to solid-state microscopic particulates.* Plasma Processes and Polymers, 2009. **6**(3): p. 170-179.